



OPEN

## Formation of the hollow nanopillar arrays through the laser-induced transformation of TiO<sub>2</sub> nanotubes

Jakub Wawrzyniak<sup>1</sup>✉, Jakub Karczewski<sup>2</sup>, Piotr Kupracz<sup>1</sup>, Katarzyna Grochowska<sup>1</sup>, Emerson Coy<sup>3</sup>, Adam Mazikowski<sup>4</sup>, Jacek Ryl<sup>5</sup> & Katarzyna Siuzdak<sup>1</sup>

In the following article, we present a simple, two-step method of creating spaced, hollow nanopillars, from the titania nanotube arrays via pulsed laser-treatment. Due to the high ordering of the structure, the prepared material exhibits photonic properties, which has been shown to increase the overall photoefficiency. The optical and morphological changes in the titania nanotubes after pulsed laser-treatment with 532, 355, and 266 nm wavelengths in the 10–50 mJ/cm<sup>2</sup> fluence range are studied. The investigation reveals, that by using appropriate wavelength and energy, the number of surface defects, geometrical features, or both can be tailored.

Due to rising worldwide energy demand and increasing awareness about the dangers of using fossil fuels, more and more attention is being paid to renewable sources of power. The titanium dioxide nanotubes (TiO<sub>2</sub>NTs) have been excessively studied for years since their first synthesis by Assefpour-Dezfily et al.<sup>1</sup> due to their excellent photocorrosion resistance<sup>2</sup>, non-toxicity, and outstanding optical properties<sup>3</sup>. Moreover, the TiO<sub>2</sub>NTs exhibit very high surface area and have easily tuneable nanotube length<sup>4</sup>, spacing<sup>5,6</sup>, and pore size<sup>7–9</sup>, all influencing properties of the nanotube array. Because of that, they have found immense success in research involving gas sensors<sup>10</sup>, filtering systems<sup>11</sup>, solar cells<sup>12</sup>, and photocatalysis<sup>13,14</sup>.

However, one of the biggest drawbacks of TiO<sub>2</sub>NTs is their wide bandgap of 3.2 eV limiting their absorption to the UV range, which represents only a small part of the solar spectrum. To successfully employ titania nanotubes in solar-driven applications, various methods of widening absorption band have been discussed in the literature. Modifications with non-metals or organics primarily focus on employing narrow bandgap materials which help in exciton generation over a broader light spectrum<sup>15,16</sup>. On the other hand, doping with noble metals, which strongly interact with light in the visible spectrum through plasmonic resonance, allows the injection of hot-electrons into nanotube arrays improving their overall photoactivity<sup>17,18</sup>.

Interestingly though, structural and morphological changes have also been shown to be a key factor in band-gap engineering<sup>19</sup>. The synthesis of TiO<sub>2</sub>NTs with the high surface-to-volume ratio results in improved radiation harvesting. Simultaneously, optimization of the length of the TiO<sub>2</sub>NTs is crucial to avoid excessive recombination of generated charge carriers<sup>20</sup>.

It should be highlighted that those methods do not rely on the incorporation of foreign atoms into the structure of titania, but rather modify existing one to broaden the absorbance spectra. It is done through so-called self-doping and relies heavily on the creation of structural defects such as oxygen vacancies and employs various methods, e.g. microwave or laser irradiation<sup>21–24</sup>. Likewise, the additional absorbance bands can be created or widened by adjusting TiO<sub>2</sub>NTs spatial distribution, similarly to how it is done in photonic structures<sup>5</sup>.

Recently, the use of titania nanotubes as photonic crystal (PC) arrays gains increased traction in literature<sup>18,25–27</sup>. Due to the high refractive index of TiO<sub>2</sub> structures, and regular spatial distribution of the nanotubes, the TiO<sub>2</sub>NTs are clear candidates for use as photonic materials. Coupled with the scattering of incident light on top of the tubular layer, the total material absorption could be greatly improved while retaining their charge percolation capabilities<sup>28–30</sup>.

<sup>1</sup>Centre of Plasma and Laser Engineering, Institute of Fluid-Flow Machinery, Polish Academy of Sciences, Fiszerka 14 st., 80-231 Gdańsk, Poland. <sup>2</sup>Department of Solid-State Physics, Gdańsk University of Technology, Gabriela Narutowicza 11/12 st., 80-233 Gdańsk, Poland. <sup>3</sup>NanoBioMedical Centre, Adam Mickiewicz University, Wszechnicy Piastowskiej 3 st., 61-614 Poznań, Poland. <sup>4</sup>Department of Metrology and Optoelectronics, Gdańsk University of Technology, Gabriela Narutowicza 11/12 st., 80-233 Gdańsk, Poland. <sup>5</sup>Department of Electrochemistry, Corrosion and Materials Engineering, Gdańsk University of Technology, Gabriela Narutowicza 11/12 st., 80-233 Gdańsk, Poland. ✉email: jwawrzyniak@imp.gda.pl

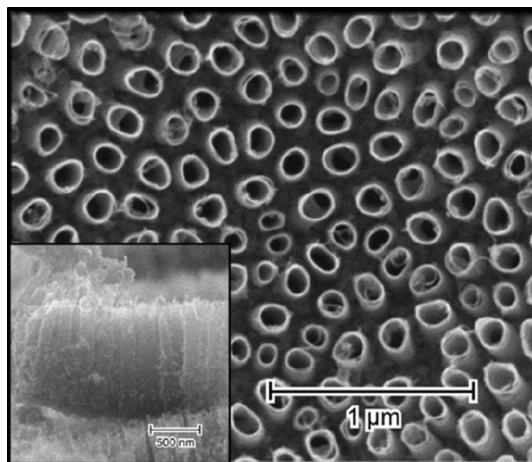


**Figure 1.** SEM image of the anodized TiO<sub>2</sub>NTs with their cross-section shown in the inset.

In our work, we present a blueprint for the creation of an array of empty, evenly spaced, self-standing TiO<sub>2</sub> nanopillars. The proposed smart laser treatment of an open tube TiO<sub>2</sub>NTs results in their closing and formation of the tight cap over the hollow tube. Although they exhibit photonic properties by themselves, they can also serve as a base for further modifications, allowing encapsulation of different materials inside, potentially serving as a shell in novel core–shell type of photonic nanostructures.

## Results and discussion

**Morphology.** As-anodized TiO<sub>2</sub>NTs have an inner radius of about 60 nm, the wall thickness of 12 nm, they are evenly distributed with the average distance between them of 70 nm, and have 1 μm in length (Fig. 1). The calcination process does not affect their morphology in any way, and they retain all their geometrical features. The effects of laser irradiation of different wavelengths within a fluence range of 10–50 mJ/cm<sup>2</sup> are presented in Fig. 2. The first column shows the effects of modification with 4th harmonics generator crystal ( $\lambda = 266$  nm), representing photon energy ( $\sim 4.6$  eV) well above the bandgap of the material ( $E_{bg} = 3.3$  eV). In the case of the lowest fluence used, no meaningful changes to TiO<sub>2</sub>NTs morphology can be observed (Fig. 2A). However, as the pulse energy rises, some nanotube tops begin to melt, forming connected platforms made of two or three closest nanotubes, resulting in non-uniform surface morphologies. Although the degree of their melting in the upper region varies clearly, the height of the TiO<sub>2</sub>NTs modified with  $\lambda = 266$  nm changes only slightly with the energy used. While TiO<sub>2</sub>NTs irradiated with 20 mJ/cm<sup>2</sup> are about 750 nm in length, those treated with 50 mJ/cm<sup>2</sup> are only about 150 nm shorter.

Considering laser-modifications with 3rd harmonics and photon energy (3.5 eV) close to the bandgap of the material, the degree of changes seems to be much more uniform across energies used (Fig. 2F–J). In the case of the lowest fluence applied, the nanotubes tops melt slightly inwards, forming half-open cylinders. Regarding fluences of 20 and 30 mJ/cm<sup>2</sup>, the upper parts of the nanotubes are fully closed and the vast majority of the nanotubes are self-standing, not merging with neighboring ones. Using higher energies results in gradually more interconnections between TiO<sub>2</sub>NTs. The nanotubes have shortened to about 840 nm after irradiation with 10 mJ/cm<sup>2</sup>, and were approximately 65 nm shorter each time the fluence was increased, down to 575 nm at 50 mJ/cm<sup>2</sup>.

Modification with photon energies (2.3 eV) much lower than the electron bandgap did not result in any changes in overall nanotubes length within the investigated range of fluences. There were, however, visible distortions in the nanotube openings when fluence 50 mJ/cm<sup>2</sup> was reached.

The TEM images confirm the empty core of the nanotubes (Fig. 3A) and show a tight cap in their upper region. Notice, that the beam has enough energy to cross the cap and reveal the internal section of the tubes. The images indicate, that the melted cap is approximately 170 nm thick, and there is still nearly 700 nm of the empty nanotube core underneath (Fig. 3D). Moreover, the evidence of the anatase crystalline phase have been found, as the Fast-Fourier Transform of the close-ups of the cap (Fig. 3B,E) reveal  $d_{(101)} = 0.35$ ,  $d_{(103)} = 0.24$ , and  $d_{(105)} = 0.17$  nm peaks (Fig. 3C,F). This shows that the majority of the anatase phase is undisturbed by laser modification.

To our knowledge, such structures have not been yet reported in the literature. Although few works regarding laser-modification of TiO<sub>2</sub>NTs are available<sup>22,23,31,32</sup>, all of the investigators have focused on the densely packed nanotube arrays, where melting of neighboring nanotubes caused their individual features to disappear. Irradiation of differently spaced nanotubes<sup>33</sup> with  $\lambda = 355$  nm and 30 mJ/cm<sup>2</sup>, however, is a reliable method of TiO<sub>2</sub>NT encapsulation (Fig. 4).

**Optical properties.** *Reflectance spectra.* The reflectance spectra for investigated samples are shown in Fig. 5. In the case of modification with  $\lambda = 266$  and 355 nm, the interference fringes can be seen. They form due to interference of the light-waves reflected from the closed, upper parts of the TiO<sub>2</sub>NTs and those propagating through the TiO<sub>2</sub>NT film, reflected at the bottom. Chiarello et al.<sup>34</sup> have proposed an equation that allows calcu-

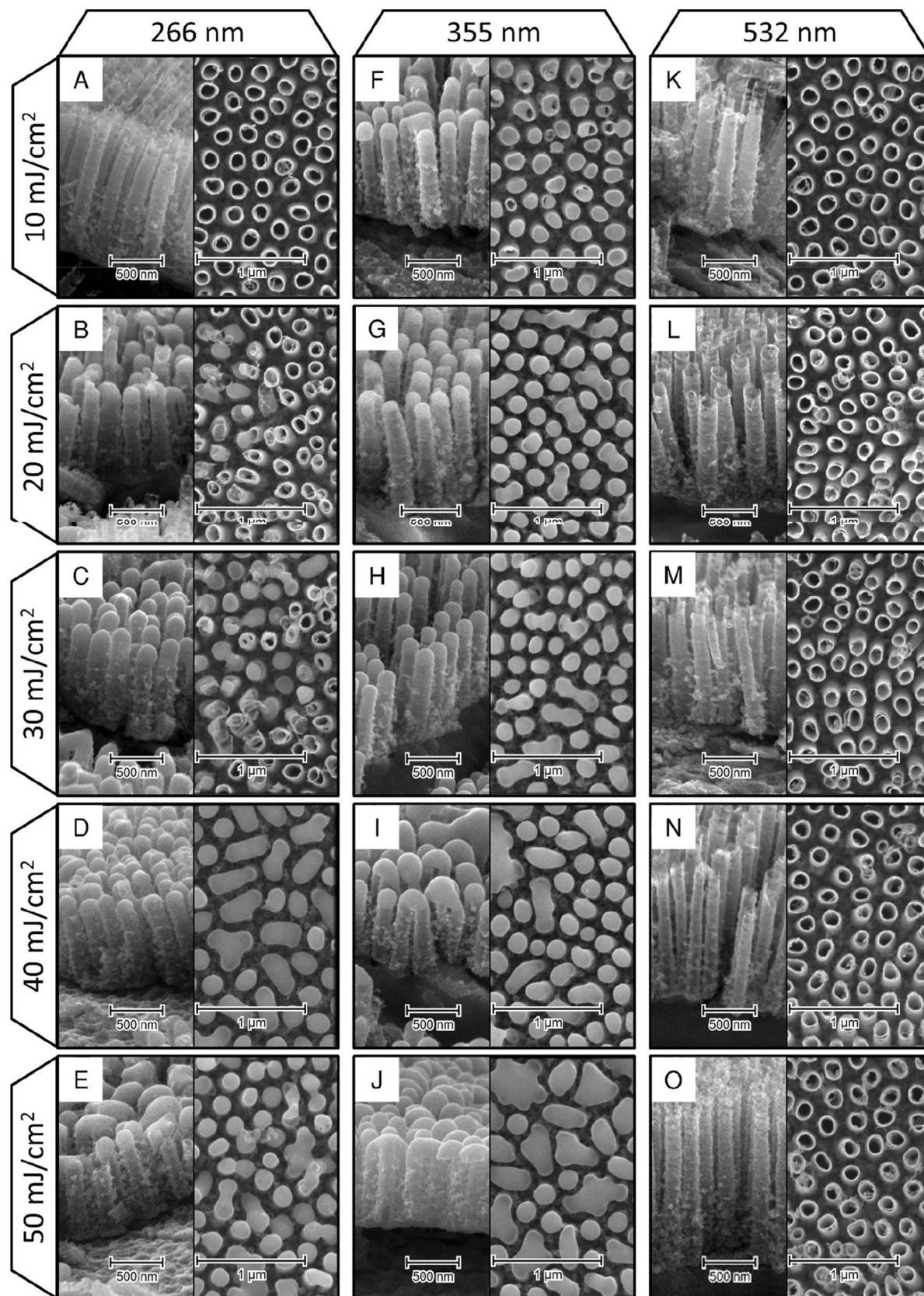


**Figure 2.** SEM images of the laser-modified  $\text{TiO}_2\text{NTs}$ . The columns show different wavelengths used (266, 355, and 532 nm respectively) while rows represent fluence used (10–50  $\text{mJ}/\text{cm}^2$ ).

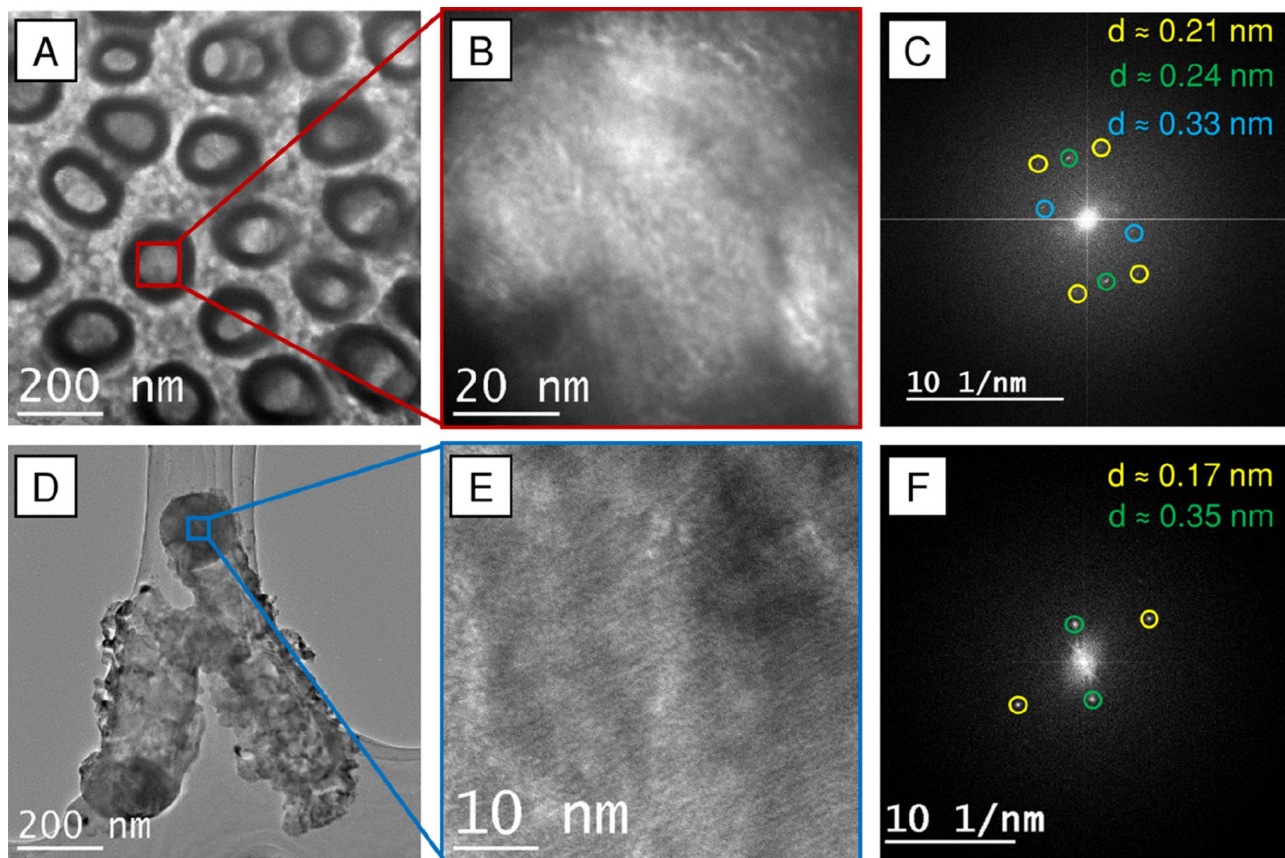


**Figure 3.** TEM images of the nanotubes irradiated with  $30 \text{ mJ/cm}^2$  with the  $\lambda = 355 \text{ nm}$ . (A) shows the top view of the  $\text{TiO}_2\text{NTs}$ . (B) Close-up of the internal section of the  $\text{TiO}_2\text{NTs}$ . (C) The FFT image of (B). (D) Shows a removed  $\text{TiO}_2\text{NT}$ , laying down on the Cu grid allowing for visualization of the cap. (E) Shows a close up of the cap and (F) the FFT image of Panel E.

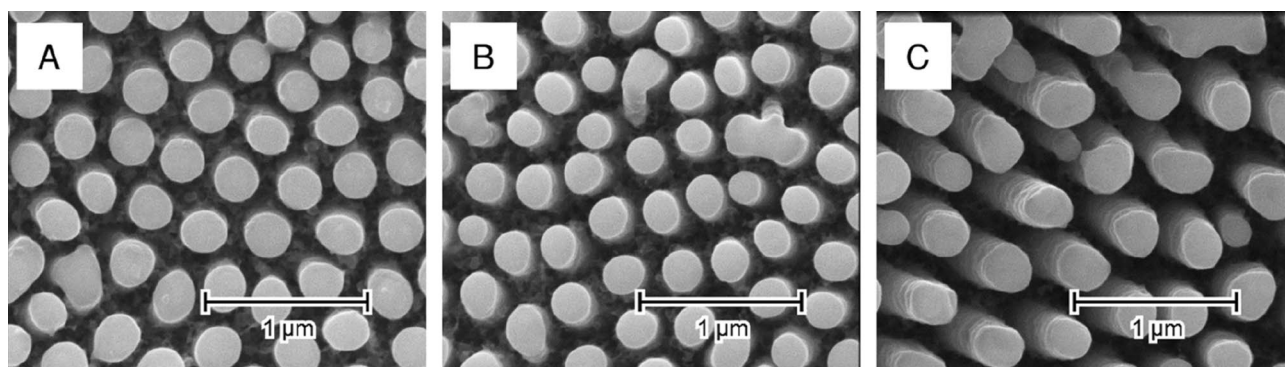


**Figure 4.** SEM images of the  $\text{TiO}_2\text{NTs}$  anodized at 40 (A), 50 (B), and 60 V (C) post laser-treatment ( $\lambda = 355 \text{ nm}$ ,  $30 \text{ mJ/cm}^2$ ).

lation of the  $\text{TiO}_2\text{NT}$  length, using two consecutive fringe positions. Regarding the irradiation at a normal angle of incidence, it can be simplified to:

$$d = \frac{\lambda_1 \lambda_2}{2n(\lambda_2 - \lambda_1)}$$

where  $d$  is the thickness of the layer,  $n$  is the refractive index of the anatase (approximately 2.2 between 450 and 600 nm), and  $\lambda_1$  and  $\lambda_2$  are the positions of the respective fringes. The equation correlates well into experimental data regarding both geometric and optical features, explaining the periodic nature of the spectrum. Moreover, the presence of the fringes or lack of thereof can be explained by the amount of the material present in the upper nanotube region, i.e. in the cap (Figs. 2, 5). The exception, in this case, would be modification with  $\lambda = 355 \text{ nm}$

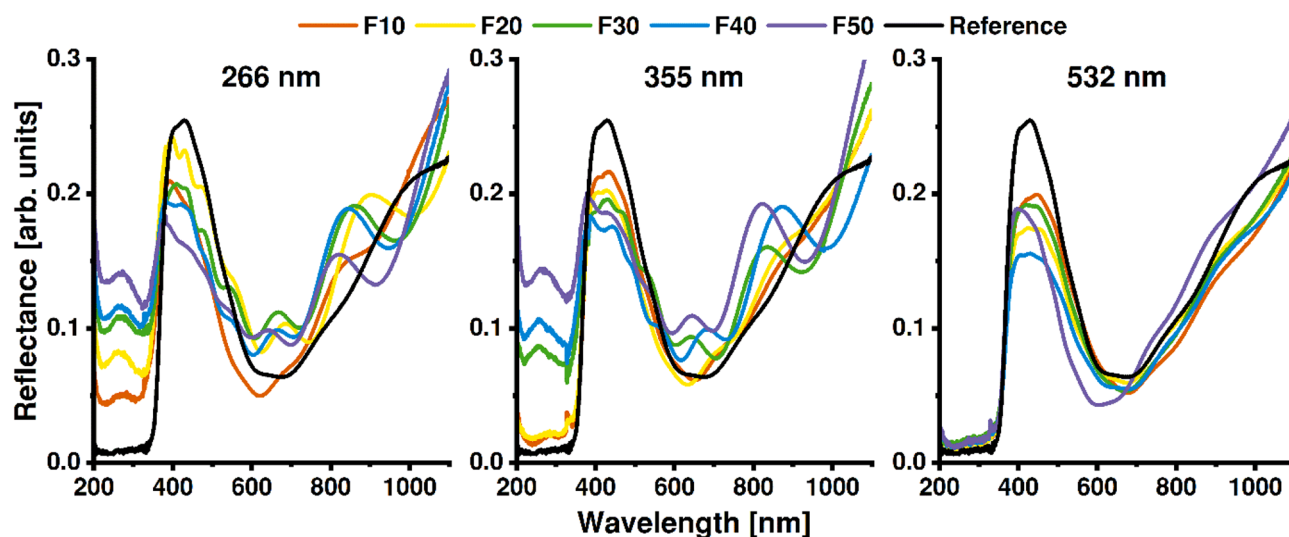


**Figure 5.** Reflectance spectra of the reference and TiO<sub>2</sub>NTs modified with three different laser wavelengths within the fluence range of 10–50 mJ/cm<sup>2</sup>.

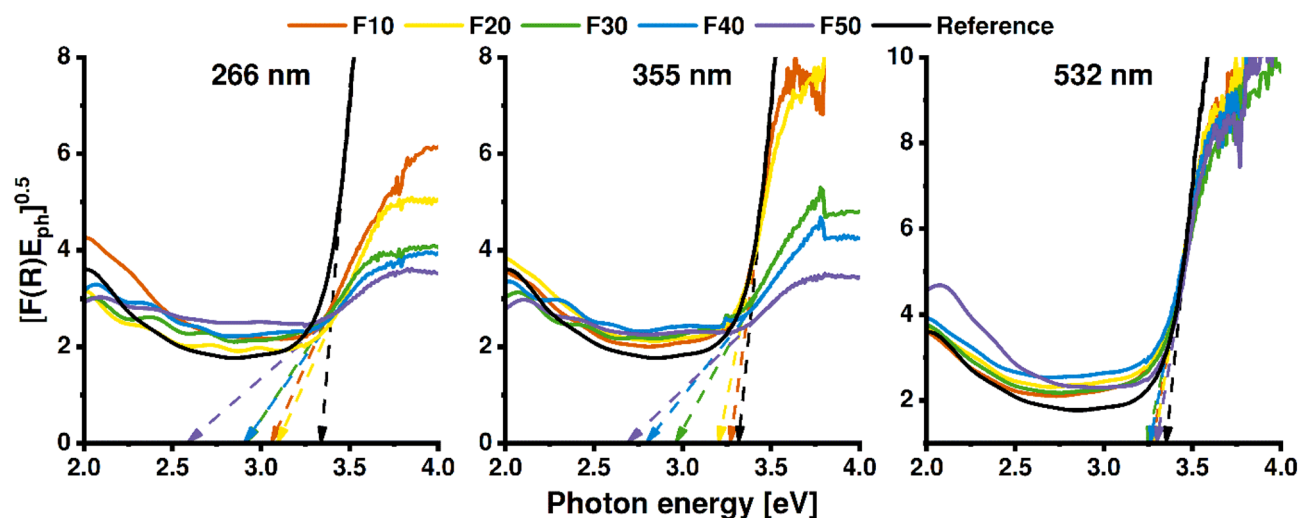


**Figure 6.** Calculated Tauc plots with dashed lines indicating bandgap values.

with 10 and 20 mJ/cm<sup>2</sup>, where although capping of the TiO<sub>2</sub>NTs is present, the periodic nature of the spectra is not distinguished. It may be explained by the very thin capping layer and a negligible amount of light reflecting from the cap. Interestingly, whereas Chiarello et al.<sup>34</sup> observed fringes for spectra recorded for TiO<sub>2</sub>NT layers as thick as 2 μm, we could not define them for the reference material with half the thickness. In this case, the defined spacing between the TiO<sub>2</sub>NTs could be the determining factor responsible for the shape of the reflectance spectra. Interestingly, the changes in the UV region of the reflectance spectra are, except fringes, unrelated to the degree of morphological changes in the TiO<sub>2</sub>NTs (see Fig. 2). An increase in the UV reflectance is present in samples irradiated with 266 and 355 nm lasers. Although in the case of irradiation with 4th harmonics the absorbance drops rapidly, slowing in the upper energy regime, a significant increase in 3rd harmonics is present only when fluence over 30 mJ/cm<sup>2</sup> is used. As the light absorption in this region is mainly attributed to the electron transitions from O<sup>2-</sup> orbital to the Ti<sup>4+</sup><sup>35</sup>, an increased presence of oxygen vacancies can result in the rise of radiative recombination seen as the increment in the reflectance spectra.

Figure 6 shows Tauc plots of the laser-modified TiO<sub>2</sub>NTs accompanied with the untreated sample. The bandgap of the reference sample equals approximately 3.3 eV, slightly higher than for bulk anatase, due to the so-called electron-confinement effect, often present in nanomaterials<sup>36–38</sup>. The  $E_{bg}$  shifts towards lower values with increased fluence for both irradiation with 266 and 355 nm, whereas it drops only slightly when the wavelength of 532 nm is applied during the modification. The narrowing of the  $E_{bg}$  values is likely related to the creation of additional localized states within the bandgap allowing lower-energy photons to be absorbed<sup>39</sup>.

**Photoluminescence.** Taking into account resolved photoluminescence (PL) spectra reported by other authors, obtained data points were fitted into distinctive emission bands (Fig. 7) using parameters listed in Table 1<sup>40–44</sup>.

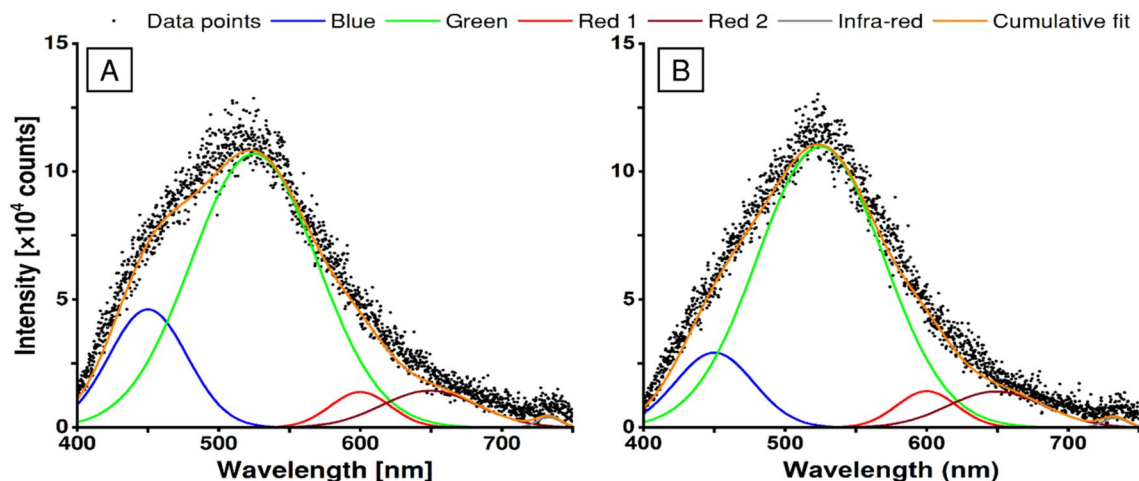


**Figure 7.** Deconvoluted photoluminescence spectra for unmodified sample (A) and the sample modified by 355 nm laser with 30 mJ/cm<sup>2</sup> (B).

| Colour             | Blue | Green | Red 1 | Red 2 | Infra-red |
|--------------------|------|-------|-------|-------|-----------|
| Peak position [nm] | 450  | 525   | 600   | 649   | 733       |
| FWHM [nm]          | 65   | 105   | 50    | 80    | 20        |

**Table 1.** Fitting parameters used to perform deconvolution of photoluminescence spectra.

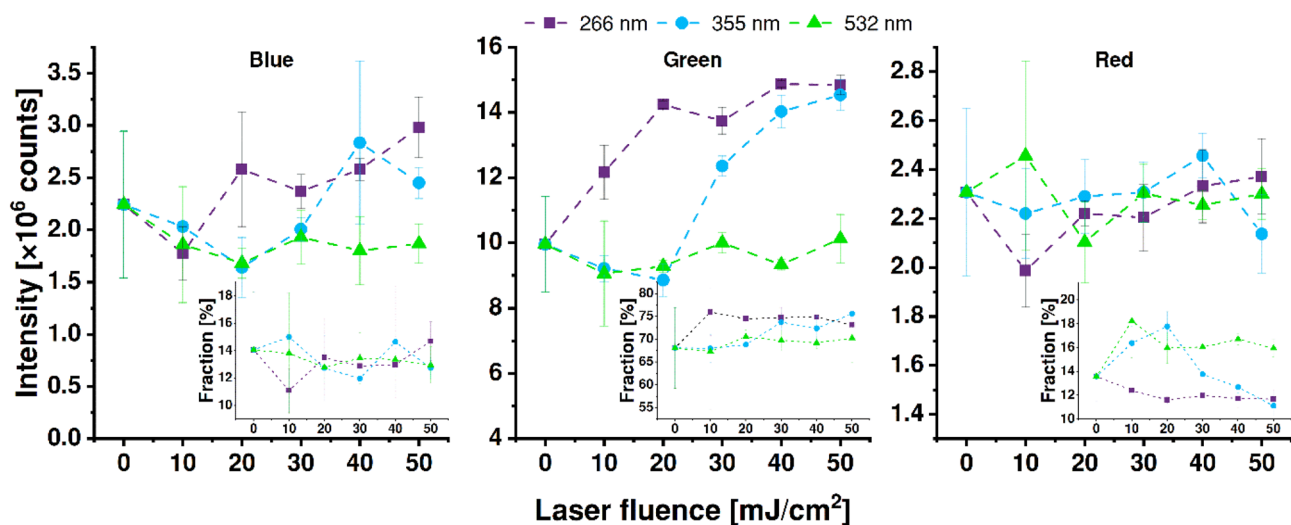


**Figure 8.** Intensities of the blue, green, and red photoluminescence of the samples as a function of laser fluence used for modification. Insets show the contribution to the total emission.

Analysis of the photoluminescence results, in general, shows that laser annealing of the TiO<sub>2</sub>NTs changes their overall emissivity spectrum. The strongest influence of laser treatment can be observed for the green light emission (Fig. 8) after irradiation of titania with 266 and 355 nm lasers. Although in the case of 4th harmonics the enhancement of emissivity is evident even when the low fluence is used, it quickly saturates at 20 mJ/cm<sup>2</sup> and a further increase in laser energy does not affect the total green emission. Changes induced by 3rd harmonics are, on the other hand, minimal for fluences up to 20 mJ/cm<sup>2</sup>, but rise and saturate at higher investigated energies. Moreover, a slight increase in the total blue emissivity was observed in the case of modification via both 3rd and 4th harmonics in their respective processing thresholds. However, none of the applied laser wavelengths modulates the red-emission sector and the usage of 2nd harmonics does not noticeably affect the emission spectrum.

In TiO<sub>2</sub>NTs, the blue photoluminescence band is related to electron–hole recombination between conduction and valence bands, green is the effect of recombination of mobile electrons with trapped holes, and red arises due to the recombination of electrons trapped on Ti<sup>3+</sup> ions with valence band<sup>44,45</sup>. Thus, the increment of the green PL

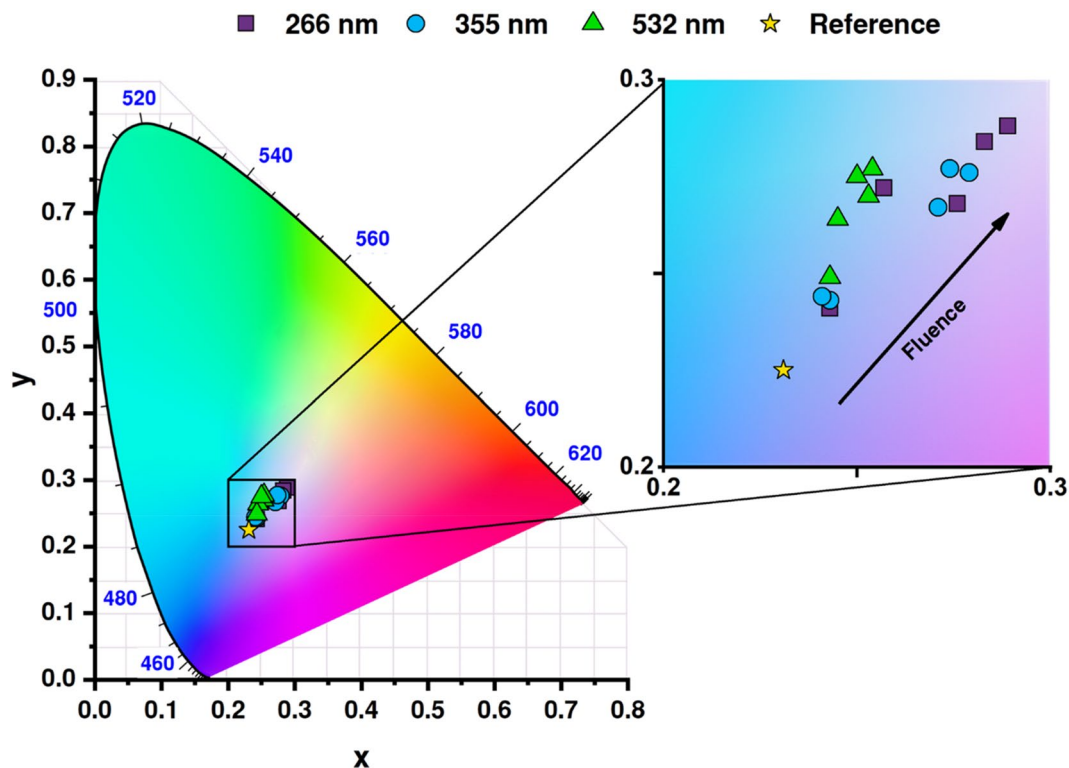


**Figure 9.** CIE xy chromaticity diagram marked with positions of investigated samples. The inset presents a close-up of the color spectrum and the arrow indicates an increase in fluence.

after the treatment with  $\lambda = 266$  and  $355$  nm may be explained by the growing number of trapped holes related to the increasing number of oxygen vacancies regarding as the tuning factor of the electronic properties of the  $\text{TiO}_2$  nanostructures<sup>46</sup>. The laser-induced increase of the number of oxygen vacancies was further confirmed by the high-resolution X-ray photoelectron spectra recorded within binding energy of  $\text{Ti}2p$  (see Figure S1 with appropriate analysis provided in ESI file)<sup>47,48</sup>.

**Colorimetry.** Apart from the typical analysis of the reflectance spectra, we performed colorimetric analysis and the results were summarized as particular points on a CIE 1931 chromaticity diagram (see Fig. 9). The colorimetric investigation lines up with previously observed effects verified via reflectance measurements. In the series representing the shortest wavelength used for titania treatment, the sample color changes rapidly towards the center of the map (white) and reaching almost the same coordinates at the high-end of measured fluence range. Modification with  $355$  nm laser pulses affects color only slightly for fluences of  $10$  and  $20$   $\text{mJ}/\text{cm}^2$ , but the skip on the CIE chart for  $30$   $\text{mJ}/\text{cm}^2$  is very definitive. Interestingly, the color is changing as well for samples modified with 2nd harmonics. Although no apparent huge shift could be observed via the naked eye, the change from the reference sample towards green color is present and saturates for fluences above  $30$   $\text{mJ}/\text{cm}^2$ . Similar behavior was found for chromium coatings after their exposure to the energetic photons from various laser sources. It confirms that laser modification could be regarded as not fully used, but a powerful tool for optical tuning of thin films<sup>49</sup>. Therefore, without the introduction of any metal or non-metal atoms to the titania structure, optimized laser treatment provides intriguing light-matter interaction behaviors.

## Conclusion

Summarizing, in the frames of this work a unique approach of obtaining free-standing, nanotube-based, hollow titania nanopillars has been shown. In the first step, self-standing titania nanotubes were fabricated via an optimized anodization process, followed by calcination which ensured crystallization. Next, three different wavelengths of a pulsed laser, namely  $266$ ,  $355$  and  $532$  nm, were used to tailor the upper part of the  $\text{TiO}_2\text{NTs}$ . Analysis of the SEM/TEM images confirms that the treatment with  $355$  nm led to the formation of crystalline caps over each hollow pillar, while the photon energies at  $266$  and  $532$  nm were either too high or too low resulting in overmelting of the nanotubes or simply preservation of their original geometry. Optical measurements reveal that materials exposed to laser radiation exhibit the nature of photonic crystal. Moreover, the increased number of oxygen vacancies with increased fluence for  $266$  and  $355$  nm wavelengths was confirmed by the photoluminescence spectra fitting approach, while colorimetric analysis indicates the possibility of color switching depending on the applied processing parameters. Obtained results strongly suggest that laser interaction with  $\text{TiO}_2$  nanotubes can lead not only to change of their geometrical features but also opens up the possibility of

tuning their optical behavior with preserving the crystalline phase and the hollow interior. To the best of our knowledge, such an approach has been shown for the very first time. Additionally, due to the chemical stability of the titania, we believe that prepared material can be adapted for many purposes, especially as a platform for encapsulation of other materials.

## Experimental section

**Sample preparation.** Titanium foil (99.7% pure, 0.127 mm thick, Strem) was cut into 35 × 25 mm pieces and degreased ultrasonically for 10 min in acetone (p.a. Protolab), ethanol (96%, Chempur) and deionized (DI) water (0.08 μS, Hydrolab) respectively. After drying in air, it was used as a working electrode in the electrochemical oxidation process to create free-standing TiO<sub>2</sub>NTs, whereas platinum net (25 × 25 mm) was used as a counter electrode. The electrolyte in which both electrodes were submerged consisted of NH<sub>4</sub>F (0.3 wt%, p.a. Chempur), HF (0.5 wt%, p.a. Chempur), and of deionized water (7.0 wt%) in diethylene glycol (p.a. Chempur). Anodization was performed at 30 V, with ramp-up and ramp-down voltages set to 0.1 V/s and controlled by in-house built hardware which was supplied by a constant voltage generator (MPS-600-5L-2). The process was performed at a constant temperature of 40 °C, controlled by a thermostat (Julabo F-12) for 2 h. After anodization, the foil was rinsed and submerged in ethanol for ca. 1 h and dried in air subsequently.

To obtain a crystalline anatase phase, the nanotubes underwent thermal treatment in the furnace (Nabertherm) at 450 °C for 2 h. While the heating rate was set to 2 °C/min, the cooling down to room temperature was performed freely overnight. A sample prepared in such a way was treated as a reference for laser-modified material.

Nd:YAG pulsed laser (6 ns, Quantel) equipped with 2nd, 3rd, and 4th harmonics generator crystals ( $\lambda = 266, 355, \text{ and } 532 \text{ nm}$ ) was used to modify the surface of TiO<sub>2</sub>NTs structure. The laser repetition rate was set to 2 Hz and its fluence to 10–50 mJ/cm<sup>2</sup>. The beam was homogenized and focused on the surface, creating 2.4 × 2.4 mm spot. The sample was placed on the motorized, computer-controlled stage (SmarAct) enabling precise movement and thus allowing modification on any part of the surface.

**Characterization.** Scanning Electron Microscope (SEM) images were taken with FE-SEM, FEI Quanta FEG 250 which was equipped with a secondary electron detector. The pictures were taken at the surface and at the cross-section in multiple places to confirm sample uniformity. During the measurements, a constant acceleration voltage of 10 kV was applied.

Transmission Electron Microscopy (TEM) investigation was done using JEOL ARM 200F, working at 80 kV. Data collected was used to confirm the crystallinity and detailed morphology of the formed nanopillars.

The UV–Vis study was done in the reflectance mode using the PerkinElmer dual-beam spectrophotometer in the range of 300–1100 nm with a scanning speed set to 120 nm/min.

Photoluminescence (PL) spectra were taken using SHAMROCK–SR-303I-A Spectrograph (Andor Technology) at room temperature. It was equipped with 450 mW LED as the excitation light source ( $\lambda = 365 \text{ nm}$ ) and ICCD camera as a detector. FGUV-11 (Thorlabs) and GG 400 (Shott AG) optical filters were used to eliminate unwanted light modes during measurements of the PL spectra. A total of 200 scans in the range of 370–800 nm were done and their average was used for further investigation. The X-ray photoelectron spectroscopy (XPS) studies were carried out using Axis Supra spectrometer equipped with monochromatic AlK $\alpha$  source with 250 μm spot diameter, and 20 eV pass energy, calibrated for adventitious carbon C1s (284.5 eV).

The colorimetric investigation was done using the Konica Minolta CS-2000 spectroradiometer, which allows for the determination of colorimetric coordinates with accuracy and repeatability of  $\pm 0.002$  according to CIE xy standard. A halogen bulb (3100 K) was used as a light source, illuminating the sample at 45°, while the measurements were taken perpendicular to the surface from a measuring field of a 1.75 mm in diameter. To become independent of the source spectral characteristics, the Konica Minolta SC-A5 white standard was used for the determination of colorimetric coordinates.

Received: 18 June 2020; Accepted: 9 November 2020

Published online: 19 November 2020

## References

- Assefpour-Dezfily, M., Vlachos, C. & Andrews, E. H. Oxide morphology and adhesive bonding on titanium surfaces. *J. Mater. Sci.* **19**, 3626–3639 (1984).
- Mahajan, V., Mohapatra, S. & Misra, M. Stability of TiO<sub>2</sub> nanotube arrays in photoelectrochemical studies. *Int. J. Hydrog. Energy* **33**, 5369–5374 (2008).
- Shi, J. *et al.* Photoluminescence characteristics of TiO<sub>2</sub> and their relationship to the photoassisted reaction of water/methanol mixture. *J. Phys. Chem. C* **111**, 693–699 (2007).
- Paulose, M. *et al.* TiO<sub>2</sub> nanotube arrays of 1000 μm length by anodization of titanium foil: Phenol red diffusion. *J. Phys. Chem. C* **111**, 14992–14997 (2007).
- Ozkan, S., Nguyen, N. T., Mazare, A. & Schmuki, P. Optimized spacing between TiO<sub>2</sub> nanotubes for enhanced light harvesting and charge transfer. *ChemElectroChem* **5**, 3183–3190 (2018).
- Ozkan, S., Mazare, A. & Schmuki, P. Critical parameters and factors in the formation of spaced TiO<sub>2</sub> nanotubes by self-organizing anodization. *Electrochim. Acta* **268**, 435–447 (2018).
- Kim, J. *et al.* Effects of NH<sub>4</sub>F and distilled water on structure of pores in TiO<sub>2</sub> nanotube arrays. *Sci. Rep.* **8**, 12487 (2018).
- Bauer, S., Kleber, S. & Schmuki, P. TiO<sub>2</sub> nanotubes: Tailoring the geometry in H<sub>3</sub>PO<sub>4</sub>/HF electrolytes. *Electrochem. Commun.* **8**, 1321–1325 (2006).
- Macak, J. M., Hildebrand, H., Marten-Jahns, U. & Schmuki, P. Mechanistic aspects and growth of large diameter self-organized TiO<sub>2</sub> nanotubes. *J. Electroanal. Chem.* **621**, 254–266 (2008).



10. Karunagaran, B., Uthirakumar, P., Chung, S. J., Velumani, S. & Suh, E.-K. TiO<sub>2</sub> thin film gas sensor for monitoring ammonia. *Mater. Charact.* **58**, 680–684 (2007).
11. Li, L. *et al.* Underwater superoleophobic porous membrane based on hierarchical TiO<sub>2</sub> nanotubes: Multifunctional integration of oil–water separation, flow-through photocatalysis and self-cleaning. *J. Mater. Chem. A* **3**, 1279–1286 (2015).
12. Wang, X., Sun, L., Zhang, S. & Wang, X. Ultralong, small-diameter TiO<sub>2</sub> nanotubes achieved by an optimized two-step anodization for efficient dye-sensitized solar cells. *ACS Appl. Mater. Interfaces* **6**, 1361–1365 (2014).
13. Kang, X. & Chen, S. Photocatalytic reduction of methylene blue by TiO<sub>2</sub> nanotube arrays: effects of TiO<sub>2</sub> crystalline phase. *J. Mater. Sci.* **45**, 2696–2702 (2010).
14. Macak, J. M., Zlamal, M., Krysa, J. & Schmuki, P. Self-organized TiO<sub>2</sub> nanotube layers as highly efficient photocatalysts. *Small* **3**, 300–304 (2007).
15. Daghrir, R., Drogui, P. & Robert, D. Modified TiO<sub>2</sub> for environmental photocatalytic applications: A review. *Ind. Eng. Chem. Res.* **52**, 3581–3599 (2013).
16. Piskunov, S. *et al.* C-, N-, S-, and Fe-doped TiO<sub>2</sub> and SrTiO<sub>3</sub> nanotubes for visible-light-driven photocatalytic water splitting: Prediction from first principles. *J. Phys. Chem. C* **119**, 18686–18696 (2015).
17. Chiarello, G. L., Aguirre, M. H. & Selli, E. Hydrogen production by photocatalytic steam reforming of methanol on noble metal-modified TiO<sub>2</sub>. *J. Catal.* **273**, 182–190 (2010).
18. Hyam, R. S. *et al.* Plasmonic–photonic interference coupling in submicrometer amorphous TiO<sub>2</sub>–Ag nanoarchitectures. *Langmuir* **33**, 12398–12403 (2017).
19. Qu, R. *et al.* Morphology-induced TiO<sub>2</sub> bandgap change for super rapid treatment of dye wastewater under visible light. *Adv. Mater. Technol.* **2**, 1700125 (2017).
20. Ghicov, A. *et al.* TiO<sub>2</sub> nanotubes in dye-sensitized solar cells: Critical factors for the conversion efficiency. *Chem. Asian J.* **4**, 520–525 (2009).
21. Zhang, Z. *et al.* Microwave-assisted self-doping of TiO<sub>2</sub> photonic crystals for efficient photoelectrochemical water splitting. *ACS Appl. Mater. Interfaces* **6**, 691–696 (2014).
22. Xu, Y., Melia, M. A., Tsui, L., Fitz-Gerald, J. M. & Zangari, G. Laser-induced surface modification at anatase TiO<sub>2</sub> nanotube array photoanodes for photoelectrochemical water oxidation. *J. Phys. Chem. C* **121**, 17121–17128 (2017).
23. Hsu, M.-Y., Van Thang, N., Wang, C. & Leu, J. Structural and morphological transformations of TiO<sub>2</sub> nanotube arrays induced by excimer laser treatment. *Thin Solid Films* **520**, 3593–3599 (2012).
24. Sopha, H. *et al.* Laser-induced crystallization of anodic TiO<sub>2</sub> nanotube layers. *RSC Adv.* **10**, 22137–22145 (2020).
25. Guo, M. *et al.* Coupling plasmonic nanoparticles with TiO<sub>2</sub> nanotube photonic crystals for enhanced dye-sensitized solar cells performance. *Electrochim. Acta* **263**, 373–381 (2018).
26. Kim, W.-T. & Choi, W.-Y. Fabrication of TiO<sub>2</sub> photonic crystal by anodic oxidation and their optical sensing properties. *Sens. Actuators A* **260**, 178–184 (2017).
27. Lu, Y., Yu, H., Chen, S., Quan, X. & Zhao, H. Integrating plasmonic nanoparticles with TiO<sub>2</sub> photonic crystal for enhancement of visible-light-driven photocatalysis. *Environ. Sci. Technol.* **46**, 1724–1730 (2012).
28. Lin, J., Liu, X., Zhu, S. & Chen, X. TiO<sub>2</sub> nanotube structures for the enhancement of photon utilization in sensitized solar cells. *Nanotechnol. Rev.* **4**, 2 (2015).
29. Waqas, M. *et al.* Multi-shelled TiO<sub>2</sub>/Fe<sub>2</sub>TiO<sub>5</sub> heterostructured hollow microspheres for enhanced solar water oxidation. *Nano Res.* **10**, 3920–3928 (2017).
30. Qi, J. *et al.* Multi-shelled CeO<sub>2</sub> hollow microspheres as superior photocatalysts for water oxidation. *Nanoscale* **6**, 4072–4077 (2014).
31. Haryński, Ł., Grochowska, K., Karczewski, J., Ryl, J. & Siuzdak, K. Scalable route toward superior photoresponse of UV-laser-treated TiO<sub>2</sub> nanotubes. *ACS Appl. Mater. Interfaces* **12**, 3225–3235 (2020).
32. Wawrzyniak, J. *et al.* Laser-assisted modification of titanium dioxide nanotubes in a tilted mode as surface modification and patterning strategy. *Appl. Surf. Sci.* **508**, 145143 (2020).
33. Wawrzyniak, J. *et al.* The geometry of free-standing titania nanotubes as a critical factor controlling their optical and photoelectrochemical performance. *Surf. Coat. Technol.* **389**, 125628 (2020).
34. Chiarello, G. L., Zuliani, A., Ceresoli, D., Martinazzo, R. & Selli, E. Exploiting the photonic crystal properties of TiO<sub>2</sub> nanotube arrays to enhance photocatalytic hydrogen production. *ACS Catal.* **6**, 1345–1353 (2016).
35. Pasikhani, J. V., Gilani, N. & Pirbazari, A. E. Improvement the wastewater purification by TiO<sub>2</sub> nanotube arrays: The effect of etching-step on the photo-generated charge carriers and photocatalytic activity of anodic TiO<sub>2</sub> nanotubes. *Solid State Sci.* **84**, 57–74 (2018).
36. Peng, H. & Li, J. Quantum confinement and electronic properties of rutile TiO<sub>2</sub> nanowires. *J. Phys. Chem. C* **112**, 20241–20245 (2008).
37. Xue, X. *et al.* Raman investigation of nanosized TiO<sub>2</sub>: Effect of crystallite size and quantum confinement. *J. Phys. Chem. C* **116**, 8792–8797 (2012).
38. Cummings, F. R., Le Roux, L. J., Mathe, M. K. & Knoesen, D. Structure induced optical properties of anodized TiO<sub>2</sub> nanotubes. *Mater. Chem. Phys.* **124**, 234–242 (2010).
39. Bharti, B., Kumar, S., Lee, H.-N. & Kumar, R. Formation of oxygen vacancies and Ti<sup>3+</sup> state in TiO<sub>2</sub> thin film and enhanced optical properties by air plasma treatment. *Sci. Rep.* **6**, 32355 (2016).
40. Mathew, S. *et al.* UV-visible photoluminescence of TiO<sub>2</sub> nanoparticles prepared by hydrothermal method. *J. Fluoresc.* **22**, 1563–1569 (2012).
41. Stevanovic, A., Büttner, M., Zhang, Z. & Yates, J. T. Photoluminescence of TiO<sub>2</sub>: Effect of UV light and adsorbed molecules on surface band structure. *J. Am. Chem. Soc.* **134**, 324–332 (2012).
42. Mercado, C., Seeley, Z., Bandyopadhyay, A., Bose, S. & McHale, J. L. Photoluminescence of dense nanocrystalline titanium dioxide thin films: Effect of doping and thickness and relation to gas sensing. *ACS Appl. Mater. Interfaces* **3**, 2281–2288 (2011).
43. Abazović, N. D. *et al.* Photoluminescence of anatase and rutile TiO<sub>2</sub> particles. *J. Phys. Chem. B* **110**, 25366–25370 (2006).
44. Pallotti, D. K., Passoni, L., Maddalena, P., Di Fonzo, F. & Lettieri, S. Photoluminescence mechanisms in anatase and rutile TiO<sub>2</sub>. *J. Phys. Chem. C* **121**, 9011–9021 (2017).
45. Jung, K. Y., Park, S. B. & Anpo, M. Photoluminescence and photoactivity of titania particles prepared by the sol–gel technique: Effect of calcination temperature. *J. Photochem. Photobiol. A* **170**, 247–252 (2005).
46. Sarkar, A. & Khan, G. G. The formation and detection techniques of oxygen vacancies in titanium oxide-based nanostructures. *Nanoscale* **11**, 3414–3444 (2019).
47. Siuzdak, K. *et al.* Thin layer of ordered boron-doped TiO<sub>2</sub> nanotubes fabricated in a novel type of electrolyte and characterized by remarkably improved photoactivity. *Appl. Surf. Sci.* **357**, 942–950 (2015).
48. Rogala, M. *et al.* Self-reduction of the native TiO<sub>2</sub> (110) surface during cooling after thermal annealing—in-operando investigations. *Sci. Rep.* **9**, 12563 (2019).
49. Kotsedi, L. *et al.* Chromium oxide formation on nanosecond and femtosecond laser irradiated thin chromium films. *Opt. Mater.* **95**, 109206 (2019).

## Acknowledgments

This work received financial support from the Polish National Science Centre: Grant No. 2017/26/E/ST5/00416. E.C acknowledges the partial support provided by the project H2020-MSCA-RISE-2017 (project number: 778157) on the TEM studies of this manuscript.

## Author contributions

J.K.—SEM investigation, P.K.—Photoluminescence investigation, E.C.—TEM investigation, A.M.—colorimetric investigation, J.R.—XPS investigation, J.W.—Uv–vis investigation, preparation of the manuscript text and figures, K.G.—research supervision, K.S.—funding acquisition, research supervision.

## Competing interests

The authors declare no competing interests.

## Additional information

**Supplementary information** is available for this paper at <https://doi.org/10.1038/s41598-020-77309-2>.

**Correspondence** and requests for materials should be addressed to J.W.

**Reprints and permissions information** is available at [www.nature.com/reprints](http://www.nature.com/reprints).

**Publisher's note** Springer Nature remains neutral with regard to jurisdictional claims in published maps and institutional affiliations.



**Open Access** This article is licensed under a Creative Commons Attribution 4.0 International License, which permits use, sharing, adaptation, distribution and reproduction in any medium or format, as long as you give appropriate credit to the original author(s) and the source, provide a link to the Creative Commons licence, and indicate if changes were made. The images or other third party material in this article are included in the article's Creative Commons licence, unless indicated otherwise in a credit line to the material. If material is not included in the article's Creative Commons licence and your intended use is not permitted by statutory regulation or exceeds the permitted use, you will need to obtain permission directly from the copyright holder. To view a copy of this licence, visit <http://creativecommons.org/licenses/by/4.0/>.

© The Author(s) 2020